

Negative grain-pressures in frictional cohesionless granular media with elongated particles

Gaël Combe^{1,*}, Bilal Al Tfaily^{2,**}, and Vincent Richefeu^{1,***}

¹Univ. Grenoble Alpes, CNRS, Grenoble INP, 3SR, 38000 Grenoble, France.

²Grande école d'ingénieurs de la construction (ESTP), Cachan, France.

Abstract. By subjecting a granular assembly to confining pressure, it is expected that each particle is compressed (positive pressure). This study highlights a situation where some particles find a mechanism to find themselves in tension (negative pressure), while the sample is compressed. This state is achieved by packing elongated rod-shaped particles in a cylindrical box and applying an uniaxial compression. Using discrete element simulations with the code `Rockable`, able to model spheropolyhedral shapes, an analysis is conducted to characterize this striking feature at first glance. The particle length are varied to show at which elongation ratio the long range interactions become sufficient to allow for friction to pull the particles, *i.e.*, make the negative grain-pressures emerge. A relation linking the orientations of negative grain-pressures to the loading direction is presented through statistical analyses.

1 Introduction

Cohesionless granular materials, when subjected to confining pressures, are typically expected to experience a positive compressive pressure, with each individual particle being compressed. However, our recent observations indicate that, under certain conditions, cohesionless frictional particles within a granular assembly can experience tensile (negative) pressure, even when the overall sample is under compression. While some studies, such as [1, 2], also report negative pressures in compressed samples, those cases involve adhesive forces between the particles, which differs from our scenario. This phenomenon, although counterintuitive, arises from the specific arrangement and interaction of particles within the system. In this study, we focus on a unique situation where elongated, rod-shaped particles are packed into a cylindrical container and subjected to uniaxial compression. Through discrete element simulations using the code `Rockable` [3], capable of modeling spheropolyhedral shapes, we investigate the conditions under which these elongated particles experience negative pressures.

The concept of tension within compressed systems, particularly in relation to the arrangement of rigid bodies, has been extensively studied in tensegrity systems [4]. Tensegrity structures, which rely on the balance of tension and compression, offer a useful analogy for understanding the mechanical behavior of granular materials in unusual stress states. In tensegrity systems, elements in compression (typically struts or rods) are held in place by a network of tensioned cables, with the system as a whole

remaining stable despite the absence of traditional internal support structures. This analogy, suggests that certain granular materials may exhibit similar behaviors, where tension and compression coexist in a manner reminiscent of tensegrity frameworks.

2 Granular model and sample preparation

This study is based on discrete element simulations. The code `Rockable`, which is a discrete element code able to model spheropolyhedral shapes, was used. The initial idea was to look at the stacking characteristics of longer and shorter rods in relation to their length. To do so, the rod-particles were shaped in a tube with round caps as sketched in Figure 1. Figure 1 defines the parametric sizes: thickness d (a constant value in the present study) and cap-to-cap length ℓ . One peculiarity of this form is that, in addition to single-point contacts at the two round-ends, multi-contact configurations can exist between the rods. Apart from that, the treatment of frictional contacts is quite classical. The normal repulsion force f_n is linear-elastic of stiffness k_n ; the tangential force intensity f_t implies an elastic stiffness $k_t = k_n$ up to a plastic yielding threshold at $|f_t| = \mu f_n$, where μ is the Coulomb friction coefficient.

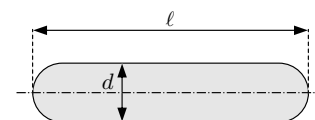


Figure 1. Sketch of the parametric sizes of the rod-particles

*e-mail: gael.combe@univ-grenoble-alpes.fr

**e-mail: baltfaily@estp.fr

***e-mail: vincent.richefeu@univ-grenoble-alpes.fr

The procedure for setting up the samples followed a well-defined protocol. In addition to defining a certain control over the arrangement at the end of preparation, its objective was also to limit the influence of the walls. The rod-particles container was thus a cylinder to avoid the rods alignment that can occur with parallelepipedic boxes and the number of rod-particles was set so that the rod length be at least 9 times smaller than the container diameter D ($D > 9\ell$) and the aspect ratio of the sample was nearly 1 to 1.5 at the end. The minimum number of rods N_p was set to 10 000.

Usually, to create a sample by gravity, the particles are arranged on a grid with random orientations in such a way that they do not overlap. However, for the longest rods, this method would result in excessive drop heights and long simulation times during the preparation. Therefore, an alternative technique was implemented using a geometric algorithm similar to the classical random close packing algorithm for spheres (this algorithm is not detailed here for the sake of brevity). A low solid fraction ($\phi \approx 0.1$) state was initially generated before allowing the rod particles to fall inside the box, with a stacking-dedicated friction coefficient of 1 (corresponding to a friction angle of 45°). To minimize the influence of the walls, the Coulomb friction between the rods and the walls was disabled. Figure 2 shows 3 examples of prepared assemblies for $\ell/d = 1.1$ (nearly spheres), $\ell/d = 6$ and $\ell/d = 10$.

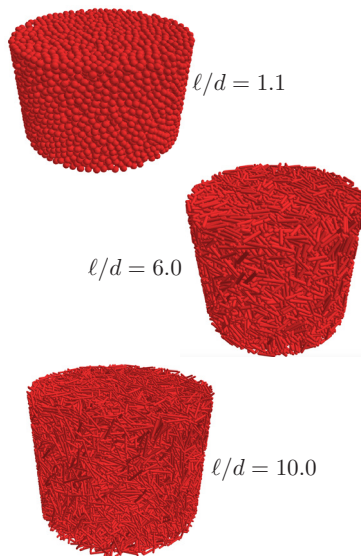


Figure 2. Example of generated assemblies.

Once built and stabilized (with gravity deactivated), the inter-rod friction was maintained at $\mu = 1$, the stiffness level $\kappa = k_n/(Pd)$ was kept constant at 1000, and the sample was subjected to axial pressure P , with no lateral deformation (oedometric conditions). The simulation was run until the contact forces were sufficiently stabilized, with stringent criteria:

- a well balanced static equilibrium of the forces $f^{j \rightarrow i}$ exerted by surrounding particles j on each particle i

$$\frac{\sum_i f^{j \rightarrow i}}{\max_i (f^{j \rightarrow i})} < 10^{-2} \quad (1)$$

- the symmetry of the moment tensors for all particles

$$\max_{i,\alpha,\beta} \left| \frac{x_\alpha^{ij} f_\beta^{j \rightarrow i} - x_\beta^{ij} f_\alpha^{j \rightarrow i}}{V_i \langle p_i \rangle} \right| < 10^{-6} \quad ; \quad (2)$$

where x_α^{ij} is the $\alpha = \{x, y, z\}$ component of the contact point coordinates between grain i and j where stands the β component of the contact force $f_\beta^{j \rightarrow i}$. V_i is the volume of the grain i , $\langle p_i \rangle$ represents the average, taken over all grains, of the mean stress acting on each grain i .

Each configuration, outlined in Table 1, defined by a single rod elongation, was simulated 3 times with different granular arrangements to increase the dataset and enhance the robustness of the subsequent analyses.

ℓ/d	N_p $\times 10^3$	ϕ ± 0.05	ℓ/d	N_p $\times 10^3$	ϕ ± 0.05
1.1	10	0.60	6.0	10	0.45
2.5	10	0.60	8.0	15	0.40
3.0	10	0.55	10.0	20	0.35

Table 1. Sample properties: number of particles N_p and solid fraction ϕ .

3 Some micro-mechanical analysis

To characterize the rod orientations resulting from the preparation protocol, as a function of the rod elongation ℓ/d , the probability distribution of the rod axis, projected on the symmetry axis \vec{y} of the sample, is plotted in Figure 3. This projection is referred to as $|\cos \gamma|$.

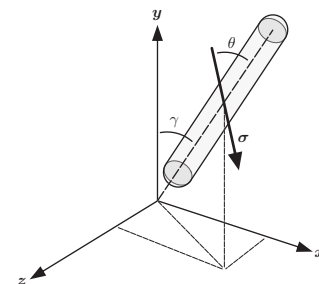


Figure 3. Definition of the orientation γ of the rod axis with respect to the vertical, and the angle θ between a given principal direction of the rod-mean-stress-tensor and the axis of the rod.

When studying the statistical distribution of orientations in three dimensions, we can represent it using a decomposition in terms of Legendre polynomials:

$$P(|\cos \gamma|) = \sum_{k=0}^{+\infty} B_{2k} P_{2k}(|\cos \gamma|) \quad (3)$$

For an expansion up to order 4, the coefficients B_2 and B_4 characterize the amplitude of the anisotropy. The orientation distribution is isotropic when $B_2 = B_4 = 0$, which corresponds to the conditions $\langle \cos^2 \gamma \rangle = \frac{1}{3}$ and $\langle \cos^4 \gamma \rangle = \frac{1}{5}$

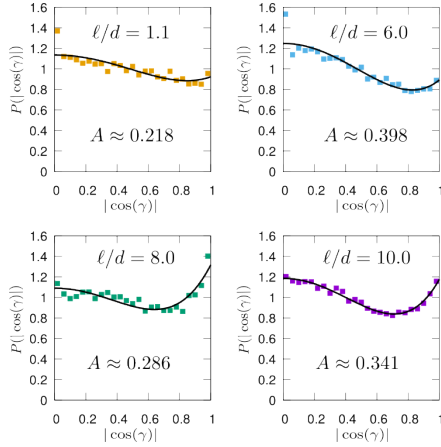


Figure 4. Probability distributions of $|\cos \gamma|$, *i.e.*, the projection of the unit vector defining the axis orientations of rods onto the vertical (see Figure 3), for different rod-elongations ℓ/d . The curve is a fit with Legendre polynomial function of order 4, where $A = \sqrt{B_2^2 + B_4^2}$ is representative of the amplitude of the orientation anisotropy.

Figure 4 presents the probability distributions of $|\cos \gamma|$, which represents the projection of the unit vector along the rod axis onto the vertical direction. The distribution is analyzed for various rod elongations, ℓ/d . The curve represents a fit using a Legendre polynomial expansion up to order 4. The coefficients $A = \sqrt{B_2^2 + B_4^2}$ quantify the degree of anisotropy in the rod orientations. A higher magnitude of these coefficients suggests stronger alignment along a preferred direction, whereas values close to zero indicate isotropic orientation.

As ℓ/d increases, we observe a transition in the distribution, with the anisotropy parameter evolving from $A \approx 0.2$ (indicative of weak anisotropy) for nearly spherical particles to $A \approx 0.4$ (moderate anisotropy) at larger elongations. This increase in anisotropy may be influenced by the cylindrical boundary of the container, despite precautions taken to ensure its diameter is nine times larger than ℓ . Nevertheless, the overall anisotropy remains relatively limited. Additionally, comparing the fitted curves with the raw data provides further insight into the accuracy of the Legendre polynomial approximation in describing the orientation distribution.

The rods are made of a tube and at each end of a sphere, whatever the elongation ℓ/d of the particle. When two particles i and j are in contact, they are in contact *via* their spheres and their tube: sphere-sphere contact, sphere-tube contact and tube-tube contact. If two rods are in contact *via* their respective spheres, the two spheres of particle i can potentially be in contact with the two spheres of grain j . In this case, the contact between the two rods is *via* two contact points, *i.e.*, the contact is double. This case is not rare and is all the more frequent as the two spheres of the

same particle are close ($\ell/d \approx 1$). For $\ell/d = 1.1$, 7 % of the contacts are double. This proportion decreases linearly with ℓ/d . It stabilizes at 3 % for $\ell/d \geq 8$.

The coordination number $\langle Z^* \rangle$ – average number of contacts carrying nonzero contact forces per particle – is influenced by the packing fraction ϕ of the granular system, as well as other factors such as the stiffness of inter-particle contacts. In static systems composed of perfectly rigid frictionless spheres, $\langle Z^* \rangle = 6$ when gravity is absent [5]. However, when inter-granular friction is considered, this value decreases below 6. For particles with complex shapes, such as clusters of spheres as in [6], the average number of contacts per cluster lacks an upper limit, as interactions between two clusters can involve multiple spheres. It follows that the number of contacts is directly related to the number of spheres constituting the clusters. To make the coordination number independent of the particle composition (spheres or tubes), we define the average number of contacts of particles in contact, $\langle Z' \rangle$, instead of $\langle Z^* \rangle$. In the simulations presented, when two rods are in contact through two contact points, only one contact is counted. For $\ell/d = 1.1$, we find that $\langle Z' \rangle \approx 4.67$, and it reaches a constant value of $\langle Z' \rangle \approx 5.74$ for $\ell/d \geq 3$. Notably, $\ell/d = 3$ appears to represent a threshold value for elongation, beyond which the inter-granular connectivity becomes independent of the particle elongation.

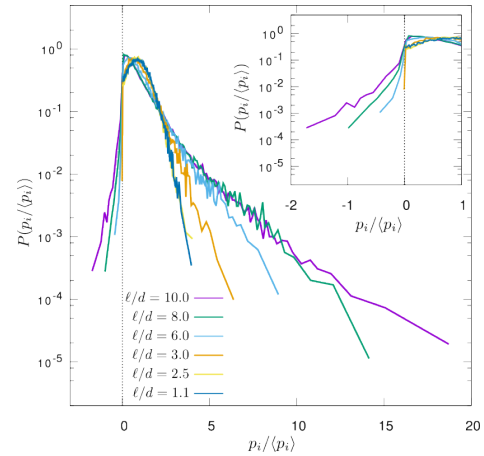


Figure 5. Probability density function of the mean normalized particle stress for different particle elongations. Negative values of $p_i/\langle p_i \rangle$ correspond to tensile stress. Note that $\langle p_i \rangle$ is positive due to the overall compressive loading. The inset shows a zoom for normalized stresses ranging from -2 to 1 . For $\ell/d = 10$, $p_i/\langle p_i \rangle < 0$ for 3% of the rod-particles.

The contacts between particles carry both normal compression and tangential forces, with the magnitudes of these forces constrained by Coulomb friction. These two components of the contact forces, defined in the local contact reference frame, can also be expressed in the global reference frame along with the coordinates of the contact points. Therefore, once the forces $f^{j \rightarrow i}$ and the contact coordinates x^{ij} are computed over the set of contacts between grain i and other grains j , they enable the calculation of the components of the stress tensor exerted on grain i . A tensorial moment for each rigid element i can be com-

puted using the following relation, and the average stress tensor is obtained by dividing the moment tensor M_i by the volume V_i of particle i

$$M_i = - \sum_{j \neq i} \mathbf{x}^{ij} \otimes \mathbf{f}^{j \rightarrow i} \quad \text{and} \quad \sigma_i = \frac{M_i}{V_i} \quad (4)$$

The symbol \otimes indicates the dyadic product. The sign convention is chosen such that compression forces are represented by positive values.

We now focus on the average stress tensor defined for each rigid rod-particle. Initially, the mean pressure is determined as the first invariant of the tensor: $p_i = \text{trace}(\sigma_i)/3$. Figure 5 presents the statistical distributions of normalized particle pressures, $p_i/\langle p_i \rangle$. The probability density function (PDF) broadens as particle elongation ℓ/d increases. For $p_i/\langle p_i \rangle > 1$, the PDFs exhibit an exponential decay, similar to normal contact forces [7]. When $\ell/d \geq 3$, the average stress can become negative, with longer particles experiencing more intense negative pressures. Conversely, for $\ell/d < 3$, pressures remain positive. This is intriguing, as in a system of purely frictional particles under compression and shear, tensile stresses can arise in sufficiently elongated particles.

As illustrated above, certain rods have been identified as experiencing tensile stresses. Here, we aim to further characterize these specific particles. To achieve this, we analyze how the principal directions of the stress tensor interact with the rod-particle axis. The first, second and third eigenvectors correspond to the principal stresses ($\sigma_1 > \sigma_2 > \sigma_3$). Figure 6 presents, for each ratio ℓ/d , the correlation between the magnitude of σ_1 (respectively σ_3) and the angle θ of the corresponding eigenvector relative to the particle axis, regardless of the spatial orientation of the stick (see Figure 3).

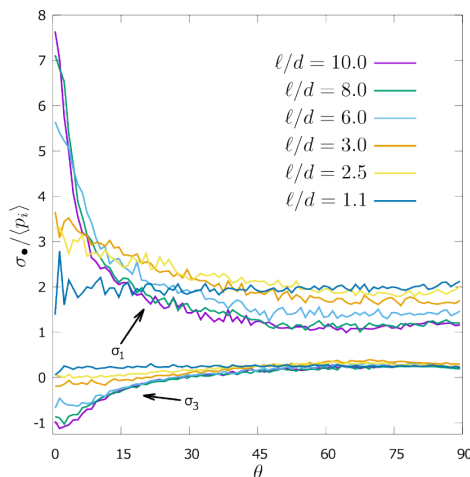


Figure 6. Averaged eigenvalues of the stress tensors (normalized by $\langle p_i \rangle > 0$) acting on each grain versus the angle θ between the eigen vector direction and the particle direction.

This figure provides several key insights. For samples composed of short rods, $\ell/d = 1.1$, we observe that $\sigma_1/\langle p_i \rangle \approx 2$ for all θ , indicating that, on average, the major principal stress does not exhibit a preferred direction along

the rods. A similar conclusion holds for σ_3 , though with a lower value of $\sigma_3/\langle p_i \rangle \approx 0.2$. However, as the particles elongate and ℓ/d increases, anisotropy emerges, becoming more pronounced with increasing particle length. This trend appears to reach a peak at $\ell/d = 8$. For $\ell/d = 8$ and $\ell/d = 10$, the conclusions remain consistent: $\sigma_1/\langle p_i \rangle$ is maximized when it acts along the longest axis of the stick, *i.e.*, for $\theta \approx 0$, indicating that particles experience stronger stress along their greatest length. Interestingly, a similar pattern is observed for σ_3 : tensile stresses are maximized at $\theta = 0^\circ$.

4 Conclusion

In this study, we investigated the emergence of negative grain pressures in packings of elongated particles subjected to uniaxial compression. Using DEM simulations, we demonstrated that as particle elongation increases, tensile stresses can develop within individual grains despite the overall compressive loading. Our results highlight a transition in stress distributions, with longer rods exhibiting a broader range of normalized pressures, including negative values. The findings provide new insights into the mechanics of granular materials with elongated shapes and suggest potential connections to tensegrity-like structural behaviors. Future work may explore the influence of additional factors such as contact parameters ($k_t/k_n, \mu$) and particle break-ability on these stress states.

Acknowledgements

The Laboratoire 3SR is part of the LabEx Tec 21 (Investissements d’Avenir, Grant Agreement No. ANR-11-LABX-0030).

References

- [1] V. Richefeu, F. Radjaï, M.E. Youssoufi, Stress transmission in wet granular materials, *Eur Phys J E Soft Matter* **21**, 359 (2006). <https://doi.org/10.1140/epje/i2006-10077-1>
- [2] T.D. Tran, S. Nezamabadi, J.P. Bayle, L. Amarid, F. Radjai, Effect of interlocking on the compressive strength of agglomerates composed of cohesive nonconvex particles, *Advanced Powder Technology* **36**, 104780 (2025). <https://doi.org/10.1016/j.appt.2025.104780>
- [3] V. Richefeu, rockable, <https://github.com/richefeu/rockable> (2025)
- [4] R. Motro, *Tensegrity: Structural Systems for the Future* (Butterworth-Heinemann, 2003), ISBN 9780080542348
- [5] I. Agnolin, J.N. Roux, Internal states of model isotropic granular packings. i. assembling process, geometry, and contact networks, *Phys. Rev. E* **76**, 061302 (2007). [10.1103/PhysRevE.76.061302](https://doi.org/10.1103/PhysRevE.76.061302)
- [6] J. Katagiri, T. Matsushima, Y. Yamada, Simple shear simulation of 3d irregularly-shaped particles by image-based dem, *Granular Matter* **12**, 491 (2010). [10.1007/s10035-010-0207-6](https://doi.org/10.1007/s10035-010-0207-6)